

Exponentially Slow Heating in Short and Long-range Interacting Floquet Systems

Francisco Machado¹, Gregory D. Meyer¹, Dominic V. Else², Chetan Nayak^{2,3}, Norman Y. Yao¹

¹*Department of Physics, University of California, Berkeley, CA 94720, USA*

²*Physics Department, University of California, Santa Barbara, CA 93106 USA*

³*Station Q, Microsoft Research, Santa Barbara, CA 93106-6105, USA*

We analyze the dynamics of periodically-driven (Floquet) Hamiltonians with short- and long-range interactions, finding clear evidence for a thermalization time, τ^* , that increases exponentially with the drive frequency. We observe this behavior, both in systems with short-ranged interactions, where our results are consistent with rigorous bounds, and in systems with long-range interactions, where such bounds do not exist at present. Using a combination of heating and entanglement dynamics, we explicitly extract the effective energy scale controlling the rate of thermalization. Finally, we demonstrate that for times shorter than τ^* , the dynamics of the system is well-approximated by evolution under a time-independent Hamiltonian D_{eff} , for both short- and long-range interacting systems.

Periodic driving is a ubiquitous tool for the controlled manipulation of quantum systems. Classic examples abound in the context of magnetic resonance spectroscopy, where a broad class of dynamical decoupling pulse sequences have been developed to suppress unwanted interactions, both within a system's own degrees of freedom, as well as with an external environment [1–7]. Periodic driving has also become a staple in the engineering toolshed of both condensed matter and atomic physics, enabling the realization of topological insulators from nominally trivial band structures [8–12] and the generation of synthetic gauge fields for neutral atoms [13–15].

When a generic system with many degrees of freedom is periodically driven, it typically absorbs energy from the driving field and heats up to an infinite temperature state [16–25], a process called thermalization [26]. However, when the driving frequency is high, the Floquet system can only absorb energy from the drive by creating multiple local excitations — an inefficient process that results in an extremely long thermalization time [27–30]. The system does *eventually* thermalize, but during the time interval before this occurs, it settles into a “prethermal” state [31–35] that exhibits the hallmarks of thermal *equilibrium*, albeit at a lower entropy than the true infinite temperature thermal state (which is only reached at very late times). In this paper, we characterize and elucidate the mechanism of Floquet thermalization.

Using massively parallel Krylov subspace methods, we explore the late time dynamics of periodically-driven spin chains with both short- and long-ranged interactions. For short-range interactions and bounded local Hilbert spaces, seminal recent results have proven that the thermalization time, τ^* , increases at least exponentially (up to log corrections) with the frequency of the drive [27–29]. We provide the first concrete demonstration of this. To this end, our results are consistent with those of [42], which also observed slow heating; but additionally, by directly observing the *exponential scaling* of the thermalization time, we can extract the effective

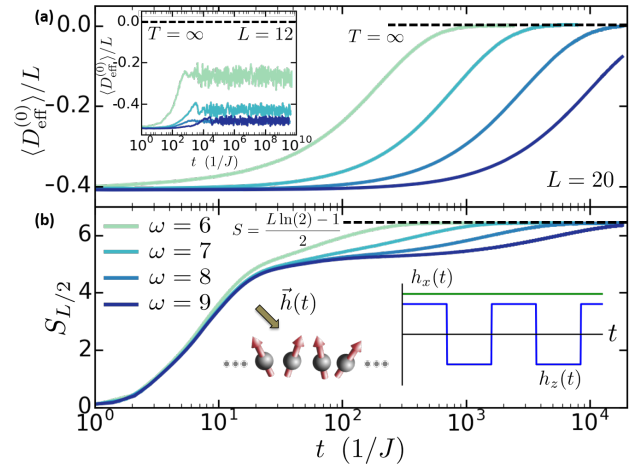


FIG. 1. Floquet thermalization dynamics of a long-range interacting spin model with $L = 20$. (a) As the driving frequency is increased, one observes an *exponential enhancement* in the time scale at which the system approaches infinite-temperature as diagnosed by the energy density, $\langle D_{\text{eff}}^{(0)} \rangle / L \rightarrow 0$. (inset) For smaller system sizes, full thermalization to infinite temperature is never observed even at late times. (b) The same exponentially slow thermalization is seen in the time scale where the half-chain entanglement entropy reaches its infinite temperature value, $\frac{L}{2} \log(2) - 0.5$. (inset) Each spin is periodically driven by a time-dependent magnetic field which exhibits a square pulse shape.

energy scale controlling the Floquet heating rate. This is enabled by going to sufficiently large system sizes such that there is a clear separation of scales between the local bandwidth and the global many-body bandwidth [43]; indeed, for driving frequencies above the many-body bandwidth, the system is trivially blocked from heating up to infinite temperature (inset, Fig. 1a). Moreover, we demonstrate that the half-chain entanglement entropy, $S_{L/2}(t)$, quickly reaches a plateau value consistent with a prethermal state before saturating to its infinite-temperature value at exponentially-late times [27–29]. On this prethermal plateau, there is an emergent

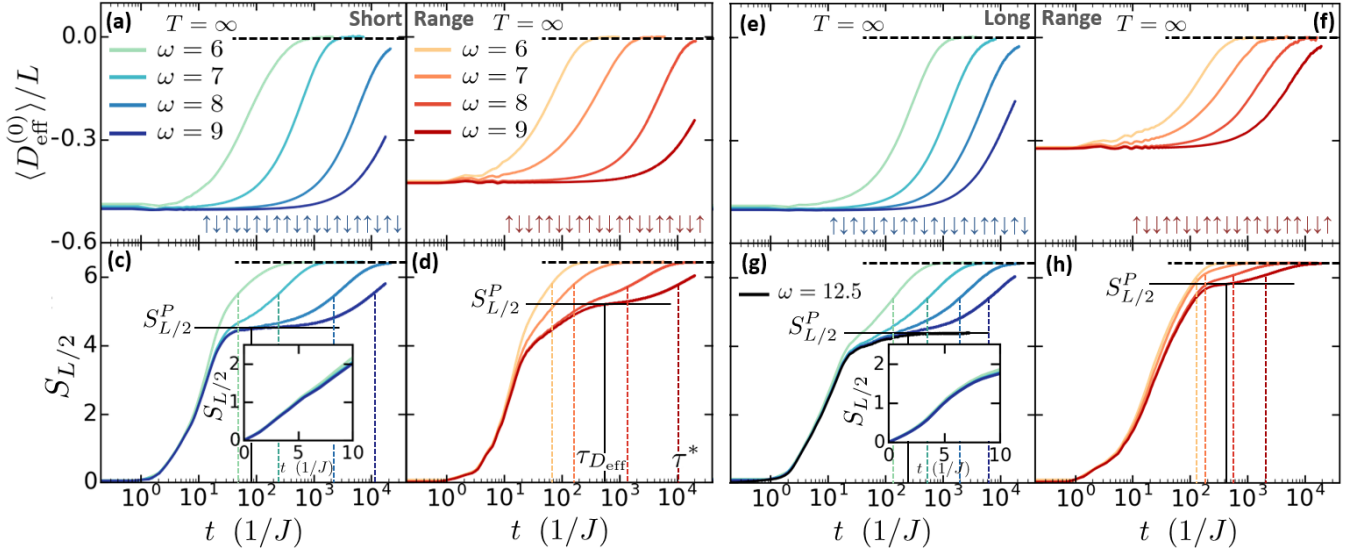


FIG. 2. Floquet evolution of both short- and long-range interacting systems with $L = 20$. a,b [e,f)] Energy density as a function of time for short-range [long-range] interactions, as measured with respect to the prethermal Hamiltonian $D_{\text{eff}}^{(0)}$ for a low temperature [a[e]] and a high temperature [b[f]] initial state. As one increases the frequency of the periodic drive, one observes an exponential increase in the thermalization time (to infinite temperature). c,d [g,h)] The half-chain entanglement entropy as a function of time for short-range [long-range] interactions. Two distinct timescales emerge: $\tau_{D_{\text{eff}}}$ and τ^* . τ^* corresponds to the thermalization time and is estimated via the colored, dashed vertical lines. $\tau_{D_{\text{eff}}}$ corresponds to the time-scale where the system reaches the prethermal Gibbs state (with entropy $S_{L/2}^P$) of the effective Hamiltonian D_{eff} , and is indicated via a solid, black vertical line. (inset, c) The initial evolution of $S_{L/2}$ is consistent with a linear light cone in the case of the short-range interactions and deviates from linear growth in the long-range case (inset, g) [36–41].

time-independent Hamiltonian, D_{eff} , that is conserved and generates the time evolution of the system at stroboscopic times $t = mT$ (where T is the period of the drive).

Finally, we also observe exponentially-long thermalization time scales (as well as an emergent D_{eff}) in a long-range, power-law interacting system, for which no bounds exist in the previous literature; such a result is particularly relevant to isolated quantum optical systems of atoms, ions and molecules, where strong interactions often take the form of long-range coulomb, dipolar, or van der Waals couplings [44–47].

Model and Probes—We analyze one-dimensional spin chains whose Floquet evolution is governed by a Hamiltonian with power-law interactions:

$$H_\ell(t) = J \sum_{i < j} \frac{\sigma_i^z \sigma_j^z}{|i - j|^\alpha} + \vec{h}(t) \cdot \left[\sum_i \vec{\sigma}_i \right] + J_x \sum_{\langle i, j \rangle} \sigma_i^x \sigma_j^x \quad (1)$$

where $\vec{h}(t) = h_x \hat{x} + (h_y \hat{y} + h_z \hat{z})(1 - 2\theta(t - T/2))$ (inset, Fig. 1b) [48], σ_i^γ are Pauli operators, $\omega = 2\pi/T$ is the driving frequency [27–29]. All energies are measured in units in which $J = 1$. We will also consider a short-range interacting model, $H_s(t)$, realized by truncating the Ising interaction in H_ℓ to nearest and next-nearest neighbor.

To characterize the Floquet thermalization dynamics, we will begin with two diagnostics (Fig. 1). First, we

will use the increase of the energy averaged over a period of the drive: $D_{\text{eff}}^{(0)} \equiv \frac{1}{T} \int_0^T dt H_\ell(t) = J \sum_{i < j} \frac{\sigma_i^z \sigma_j^z}{|i - j|^\alpha} + h_x \sum_i \sigma_x + J_x \sum_{\langle i, j \rangle} \sigma_x^i \sigma_x^j$ [49]; we note that $D_{\text{eff}}^{(0)}$ is actually the first term in an expansion for the prethermal Hamiltonian, $D_{\text{eff}} = D_{\text{eff}}^{(0)} + D_{\text{eff}}^{(1)}/\omega + D_{\text{eff}}^{(2)}/\omega^2 + \dots$, which contains a finite but exponentially-large number of terms [27, 28]. To set notation, let us also define $\mathcal{D}_{\text{eff}}^n$ as the truncation of D_{eff} to n -th order in $1/\omega$. As a second diagnostic, we will investigate the growth of the half-chain entanglement entropy as a function of time: $S_{L/2} \equiv -\text{Tr}(\rho_{L/2} \ln \rho_{L/2})$ where $\rho_{L/2} \equiv \text{Tr}_{1 \leq i \leq L/2}(|\psi(t)\rangle\langle\psi(t)|)$.

Exponentially slow thermalization—We directly compute the Floquet evolution of up to $L = 22$ spins using massively parallel Krylov subspace techniques [50–52]. We consider initial product states with spins polarized along \hat{z} and control the energy density of the initial state by varying the number of equally-spaced domain walls that are present. We begin with the short-range model, $H_s(t)$ and compute the time evolution of $\langle D_{\text{eff}}^{(0)}(t) \rangle / L$ for $L = 20$ spins at a variety of driving frequencies (significantly larger than the local energy scales of the Hamiltonian but smaller than the global many-body bandwidth [53]). Unlike the small size ($L = 12$) exact diagonalization (ED) results (inset, Fig. 1a), one observes a clear approach to infinite temperature ($\langle D_{\text{eff}}^{(0)} \rangle / L \rightarrow 0$) at late

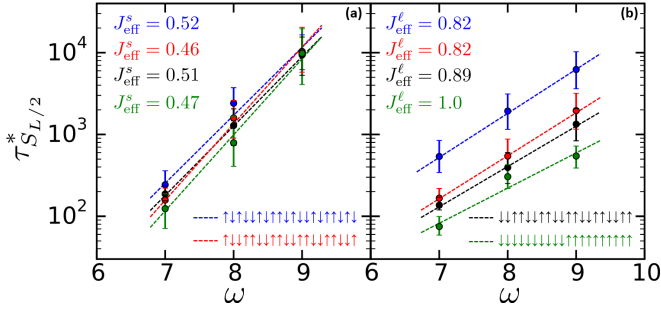


FIG. 3. The thermalization time τ^* , as extracted from $S_{L/2}$, as a function of driving frequency for both (a) short- and (b) long-range interactions. The slope provides a direct estimate of J_{eff} , the energy scale, controlling the slow thermalization dynamics. The extracted J_{eff} is largely independent of initial state (different colors) and is consistent with its interpretation as an effective local energy scale of the system. Initial states near the edge of the spectrum exhibit slightly larger τ^* , which can be qualitatively attributed to a reduction of the density of states at these energies.

times, as shown in Fig. 2a. We define the thermalization time τ^* as the time at which the energy density is halfway from its initial value to its infinite temperature value, so that τ^* is defined by, $\langle D_{\text{eff}}^{(0)}(\tau^*) \rangle = 0.5 \langle D_{\text{eff}}^{(0)}(t=0) \rangle$. For both low (Fig. 2a) and high temperature (Fig. 2b) initial states, one observes an exponential enhancement of τ^* as a function of increasing driving frequency.

To further probe the exponentially slow heating of the system, we investigate the growth of the half-chain entanglement entropy as a function of time. We expect the evolution of $S_{L/2}(t)$ to be characterized by three distinct regimes: an initial growth period beginning from $S_{L/2}(0) = 0$; an intermediate plateau where the entropy reaches its prethermal value, $S_{L/2}^P$; and a final plateau once the system has fully thermalized to infinite temperature, with $S_{L/2} = (L \ln(2) - 1)/2$ [54]. This is indeed born out by the numerics (Fig. 2c,d). The time scale at which the entropy is halfway from its prethermal plateau value to its infinite temperature value gives us an alternate definition of τ^* , $S_{L/2}(\tau^*) = S_{L/2}^P + [(L \ln(2) - 1)/2 - S_{L/2}^P]/2$, and has the virtue of not relying upon a choice of operator (such as $\mathcal{D}_{\text{eff}}^n$) used to probe the state of the system. For both low (Fig. 2c) and high (Fig. 2d) temperature initial states, one observes an exponentially-long heating time scale consistent with that extracted from $\langle D_{\text{eff}}^{(0)} \rangle / L$. To this end, Fig. 3a shows just how well τ^* fits an exponential dependence for a variety of different initial states.

There is a second time scale in the problem; namely, the time, $\tau_{D_{\text{eff}}}$, at which the entanglement entropy reaches its prethermal plateau value, $S_{L/2}^P$, as depicted in Fig. 2c,d. This is the time at which the system *globally* establishes the prethermal equilibrium-like Gibbs state of D_{eff} and is expected to be greater than the *local* thermalization time of D_{eff} by a factor of order $\sim L$. The value

of the plateau entropy, $S_{L/2}^P$, depends on the inverse temperature of the prethermal ensemble, β_{eff} , which in turn can be directly estimated using the energy density, ϵ , of the initial state: $\epsilon L = \langle D_{\text{eff}}(t=0) \rangle \approx \text{Tr} [D_{\text{eff}} e^{-\beta_{\text{eff}} D_{\text{eff}}}]$.

To quantitatively verify this relationship, we utilize small size exact diagonalization results on $\mathcal{D}_{\text{eff}}^4$ in order to estimate the entanglement entropy as a function of inverse temperature [55]. In the case of short-range interactions, this approach predicts $S_{L/2}^P = 4.6 \pm 0.4$ and $S_{L/2}^P = 5.4 \pm 0.5$ for low and high temperature initial states, respectively, both in excellent agreement with the numerically observed plateau (Fig. 2c,d). For long-range interactions, we find that finite size effects in the ED prevent an accurate extrapolation of the entropy and lead to systematic overestimate of the plateau entropy [55].

We now turn to the long-range interacting model, $H_\ell(t)$, with power-law $\alpha = 1.25$, where we again compute $\langle D_{\text{eff}}^{(0)}(t) \rangle / L$ and $S_{L/2}(t)$. We note that the recent proofs [27–29] of exponentially-slow heating in Floquet systems seem to be naturally extendable to the case of long-range few-body interactions, such as the power-law two-body interactions in Eqn. (1). The intuition is that the system still needs to make many rearrangements, each with a few-body (albeit long-ranged) interaction, in order to absorb energy ω from the drive. Indeed, for both low (Fig. 2e,g) and high (Fig. 2f,h) temperature initial states, we observe exponentially slow heating times as a function of frequency, analogous to the short-range case.

A few remarks are in order. First, we note that in the long-range model, the early-time entanglement entropy exhibits a more complex light cone, deviating from the linear one observed in the short-ranged case (inset, Fig. 2c,g). Second, for the same frequencies at which there is already a clear plateau in the short-ranged model, the long-range system exhibits a shoulder with a weak up-slope, which only flattens into a true plateau for larger frequencies (Fig. 2g). Third, while both the short- and long-range systems exhibit exponentially slow thermalization, there is a clear quantitative difference between the heating rates in the two cases.

To further explore this, we directly extract the energy scale controlling the exponentially slow heating (i.e. the effective local bandwidth), by fitting τ^* (extracted from $S_{L/2}$) to $\tau^* \sim e^{\omega/J_{\text{eff}}}$, as depicted in Fig. 3. In the case of short-range interactions, both low and high temperature initial states give $J_{\text{eff}}^s \approx 0.5 \pm 0.1$, consistent with the strength of terms in $H_s(t)$. For the long-range interacting model, one finds a larger $J_{\text{eff}}^l \approx 0.9 \pm 0.1$. Intriguingly, these heating rates yield a ratio, $J_{\text{eff}}^l/J_{\text{eff}}^s \approx 1.8 \pm 0.2$, which is consistent with the ratio of the average strength of all interactions emanating from each site, $[\sum |i-j|^{-1.25}] / [1 + 2^{-1.25}] \approx 1.6$ [56]. We note that the prefactor of the exponential in τ^* is larger for initial states near the edges of the spectrum, which could arise from the smaller density of states there (Fig. 3) [55].

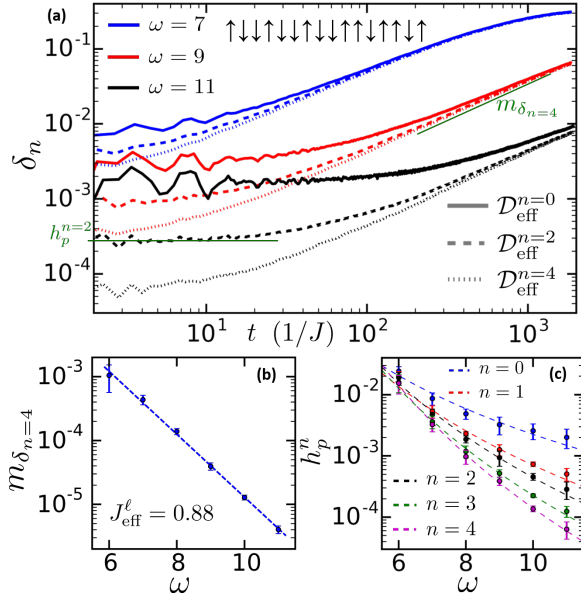


FIG. 4. a) The difference, δ_n , of the expectation value of $\mathcal{O} = D_{\text{eff}}^{(0)}/L$ as a function of time, for a chain of length $L = 16$, with different frequencies (colors) and different Magnus truncation orders (line style). The distinct regimes are seen: an initial plateau at short times and a linear increase at late times. b) Extracted slope of the late time linear regime of δ_n as a function of frequency. This provides an independent estimate for J_{eff}^ℓ which is in excellent agreement with that calculated from $\tau_{S_{L/2}}^*$. c) Plateau height $h_p^{(n)}$ for different Magnus truncation orders, n , as a function of frequency. The results are consistent with an n -dependent power law.

Long-range prethermal effective Hamiltonian—We now demonstrate that the time-independent prethermal Hamiltonian D_{eff} is indeed the generator of Floquet dynamics at stroboscopic times up to τ^* . Here, we will focus on the more surprising long-range case, leaving the short-range case for the supplementary information [55]. Unlike the question of slow heating, a proof of the existence of a time-independent D_{eff} may need to employ Lieb-Robinson bounds for long-range interactions [36–41], for which the tightest possible bounds may not yet have been found for $d < \alpha < 2d$, where d is the spatial dimension. As aforementioned, we not only observe the same exponentially-slow approach to the maximum entropy (consistent with $\langle D_{\text{eff}}^{(0)}(t) \rangle / L$), but also the presence of a prethermal plateau (for both low and high temperature initial states), indicative of the existence of D_{eff} even for long-range interacting systems (Fig. 2g,h)!

Further evidence for the existence of a time-independent D_{eff} comes from comparing the system's evolution under the full Floquet unitary, $U_f \equiv e^{-i \int_0^T H_I(t) dt}$, to evolutions under truncations of the Magnus expansion: $D_{\text{eff}} = D_{\text{eff}}^{(0)} + D_{\text{eff}}^{(1)}/\omega + D_{\text{eff}}^{(2)}/\omega^2 + \dots$ at leading order ($D_{\text{eff}}^{(0)}$), at second order ($D_{\text{eff}}^{(2)}$), and at fourth order ($D_{\text{eff}}^{(4)}$).

In Fig. 4a, we plot $\delta_n = |\langle \mathcal{O} \rangle_{U_f} - \langle \mathcal{O} \rangle_{D_{\text{eff}}^{(n)}}|$, as a function of time for different frequencies and different Magnus truncation orders, with operator $\mathcal{O} = D_{\text{eff}}^{(0)}/L$ (other choices of local operators exhibit similar results but this one has the cleanest numerics [55]). Here, $\langle \mathcal{O} \rangle_H$ is the expectation value of \mathcal{O} evolved under H ; thus, $\delta_n(t)$ captures the time-dependent difference in the expectation value of \mathcal{O} evolved under the full Floquet unitary versus under different approximations to D_{eff} . Inspection reveals two essential features: a short-time plateau [57] whose value depends on both n and ω , followed by linear growth at late times that seems to converge for the different truncation orders. To understand these features, we note that there are two contributions to $\delta_n(t)$.

First, since D_{eff} approximates the full Floquet evolution only up to a time scale $\tau^* \sim e^{\omega/J_{\text{eff}}}$, one expects the exponentially slow accumulation of errors, $\delta \sim te^{-\omega/J_{\text{eff}}}$. Second, even at short times, one expects a finite discrepancy to arise simply from the fact that the n^{th} order Magnus approximation still differs from D_{eff} (e.g. by terms such as $D_{\text{eff}}^{(n+1)}/\omega^{n+1} + D_{\text{eff}}^{(n+2)}/\omega^{n+2} + \dots$). This second point explains the qualitative dependence of the plateau value on n and ω . In particular, larger n and larger ω both lead to a smaller initial plateau for $\delta_n(t)$ since they correspond to decreasing the effect of higher-order terms in the expansion; by measuring the plateau height h_p as a function of frequency, we find that it is consistent with $h_p \sim \omega^{-\gamma(n)}$, where γ is an n -dependent power-law (Fig. 4c).

Finally, the observed linear growth of $\delta_n(t)$ at late times is consistent with the exponentially slow accumulation of errors, $\delta \sim te^{-\omega/J_{\text{eff}}}$, and enables another independent extraction of J_{eff} . In particular, as shown in Fig. 4b, by plotting the slope of the late time growth of $\delta_n(t)$ as a function of the frequency, one obtains $J_{\text{eff}} \approx 0.88 \pm 0.05$ consistent with that calculated from the entanglement entropy in Fig. 3.

Conclusion—Despite their ubiquity, periodically-driven Floquet systems have generally not shown distinct phases of matter. This is largely due to their tendency to heat up to infinite temperature, except in certain exceptional cases, such as free fermion systems (e.g. topological insulators [8–12]), and strongly-disordered one-dimensional (and possibly, two-dimensional) systems in the many-body localized phase [58–63]. In the high-frequency limit, however, we have shown that there is an exponentially-long time interval during which a system may, as it would in true thermal equilibrium, realize phases of matter and phase transitions between them, including certain phases that do not exist in undriven systems [29, 64, 65].

On the experimental side, prethermalization provides a straightforward technique for extending the thermalization time-scales of Floquet systems. This enables experiments to work in parallel with theory in realizing and

studying novel out-of-equilibrium phases. This formalism also enables the engineering of quantum evolution similar to dynamical decoupling and other techniques more common in the magnetic resonance community.

We gratefully acknowledge the insights of and discussions with E. Altman, B. Bauer, M. Bukov, P. Hess, V. Khemani, C. Monroe, M. Zaletel, J. Zhang. This work was supported, in part by, the NSF PHY-1654740, the Miller Institute for Basic Research in Science, and the LDRD Program of LBNL under US DOE Contract No. DE-AC02-05CH11231. D.V.E. is supported by the Microsoft Corporation.

-
- [1] C. P. Slichter, *Principles of magnetic resonance*, Vol. 1 (Springer Science & Business Media, 2013).
 - [2] E. L. Hahn, *Physical review* **80**, 580 (1950).
 - [3] J. Waugh, L. Huber, and U. Haeberlen, *Physical Review Letters* **20**, 180 (1968).
 - [4] W. Rhim, A. Pines, and J. Waugh, *Physical Review B* **3**, 684 (1971).
 - [5] W.-K. Rhim, D. Elleman, and R. Vaughan, *The Journal of Chemical Physics* **59**, 3740 (1973).
 - [6] L. Viola, E. Knill, and S. Lloyd, *Physical Review Letters* **82**, 2417 (1999).
 - [7] L. M. Vandersypen and I. L. Chuang, *Reviews of modern physics* **76**, 1037 (2005).
 - [8] J.-I. Inoue and A. Tanaka, *Physical Review Letters* **105**, 017401 (2010), arXiv:1006.5283 [cond-mat.mtrl-sci].
 - [9] N. H. Lindner, G. Refael, and V. Galitski, *Nat. Phys.* **7**, 490 (2011).
 - [10] Y. H. Wang, H. Steinberg, P. Jarillo-Herrero, and N. Gedik, *Science* **342**, 453 (2013), arXiv:1310.7563 [cond-mat.mes-hall].
 - [11] L. Jiang, T. Kitagawa, J. Alicea, A. R. Akhmerov, D. Pekker, G. Refael, J. I. Cirac, E. Demler, M. D. Lukin, and P. Zoller, *Physical Review Letters* **106**, 220402 (2011), arXiv:1102.5367 [cond-mat.quant-gas].
 - [12] M. Thakurathi, A. A. Patel, D. Sen, and A. Dutta, *Phys. Rev. B* **88**, 155133 (2013), arXiv:1303.2300 [cond-mat.mes-hall].
 - [13] D. Jaksch and P. Zoller, *New Journal of Physics* **5**, 56 (2003).
 - [14] V. Galitski and I. B. Spielman, *Nature* **494**, 49 (2013).
 - [15] N. Goldman, G. Juzeliūnas, P. Öhberg, and I. B. Spielman, *Reports on Progress in Physics* **77**, 126401 (2014).
 - [16] T. Prosen, *Physical review letters* **80**, 1808 (1998).
 - [17] T. Prosen, *Physical Review E* **60**, 3949 (1999).
 - [18] L. D'Alessio and A. Polkovnikov, *Annals of Physics* **333**, 19 (2013).
 - [19] A. Lazarides, A. Das, and R. Moessner, *Physical Review E* **90**, 012110 (2014).
 - [20] L. D'Alessio and M. Rigol, *Phys. Rev. X* **4**, 041048 (2014).
 - [21] M. Bukov, L. D'Alessio, and A. Polkovnikov, *Advances in Physics* **64**, 139 (2015).
 - [22] P. Ponte, A. Chandran, Z. Papić, and D. A. Abanin, *Annals of Physics* **353**, 196 (2015).
 - [23] M. Bukov, S. Gopalakrishnan, M. Knap, and E. Demler, *Phys. Rev. Lett.* **115**, 205301 (2015).
 - [24] S. A. Weidinger and M. Knap, *Scientific Reports* **7**, 45382 (2017).
 - [25] D. J. Luitz, Y. B. Lev, and A. Lazarides, (2017), arXiv:1706.09429.
 - [26] The analogous phenomenon in undriven systems is the evolution of a generic state into a thermal state.
 - [27] D. A. Abanin, W. De Roeck, and F. Huveneers, *Physical review letters* **115**, 256803 (2015).
 - [28] D. Abanin, W. De Roeck, W. W. Ho, and F. Huveneers, *Communications in Mathematical Physics*, 1 (2015).
 - [29] D. V. Else, B. Bauer, and C. Nayak, *Physical Review X* **7**, 011026 (2017).
 - [30] D. A. Abanin, W. De Roeck, W. W. Ho, and F. Huveneers, *Physical Review B* **95**, 014112 (2017).
 - [31] J. Berges, S. Borsányi, and C. Wetterich, *Physical review letters* **93**, 142002 (2004).
 - [32] M. Moeckel and S. Kehrein, *Physical review letters* **100**, 175702 (2008).
 - [33] M. Gring, M. Kuhnert, T. Langen, T. Kitagawa, B. Rauer, M. Schreitl, I. Mazets, D. A. Smith, E. Demler, and J. Schmiedmayer, *Science* **337**, 1318 (2012).
 - [34] M. Marcuzzi, J. Marino, A. Gambassi, and A. Silva, *Physical review letters* **111**, 197203 (2013).
 - [35] F. Essler, S. Kehrein, S. Manmana, and N. Robinson, *Physical Review B* **89**, 165104 (2014).
 - [36] M. B. Hastings and T. Koma, *Communications in mathematical physics* **265**, 781 (2006).
 - [37] P. Hauke and L. Tagliacozzo, *Physical review letters* **111**, 207202 (2013).
 - [38] J. Eisert, M. van den Worm, S. R. Manmana, and M. Kastner, *Physical review letters* **111**, 260401 (2013).
 - [39] Z.-X. Gong, M. Foss-Feig, S. Michalakakis, and A. V. Gorshkov, *Physical review letters* **113**, 030602 (2014).
 - [40] M. Foss-Feig, Z.-X. Gong, C. W. Clark, and A. V. Gorshkov, *Physical review letters* **114**, 157201 (2015).
 - [41] T. Matsuta, T. Koma, and S. Nakamura, *Annales Henri Poincaré* **18**, 519 (2017).
 - [42] M. Bukov, M. Heyl, D. A. Huse, and A. Polkovnikov, *Physical Review B* **93**, 155132 (2016).
 - [43] The global bandwidth is infinite in the thermodynamic limit, but finite in a finite system size.
 - [44] B. Yan, S. A. Moses, B. Gadway, J. P. Covey, K. R. Hazzard, A. M. Rey, D. S. Jin, and J. Ye, *Nature* **501**, 521 (2013).
 - [45] J. Zeiher, J.-y. Choi, A. Rubio-Abadal, T. Pohl, R. van Bijnen, I. Bloch, and C. Gross, arXiv preprint arXiv:1705.08372 (2017).
 - [46] M. G. Dutt, L. Childress, L. Jiang, E. Togan, J. Maze, F. Jelezko, A. Zibrov, P. Hemmer, and M. Lukin, *Science* **316**, 1312 (2007).
 - [47] C. Schneider, D. Porras, and T. Schaetz, *Reports on Progress in Physics* **75**, 024401 (2012).
 - [48] The parameters used for the remainder of the manuscript are: $J = 1$, $J_x = 0.19$, $h_x = 0.21$, $h_y = 0.17$, $h_z = 0.13$, $\alpha = 1.25$.
 - [49] In the short-range case, $D_{\text{eff}}^{(0)}$ will of course only contain the nearest and next nearest neighbor Ising terms.
 - [50] V. Hernandez, J. E. Roman, and V. Vidal, *ACM Trans. Math. Software* **31**, 351 (2005).
 - [51] J. E. Roman, C. Campos, E. Romero, and A. Tomas, *SLEPc Users Manual*, Tech. Rep. DSIC-II/24/02 - Revision 3.7 (D. Sistemes Informàtics i Computació, Universitat Politècnica de València, 2016).
 - [52] S. Balay, W. D. Gropp, L. C. McInnes, and B. F. Smith,

- in *Modern Software Tools in Scientific Computing*, edited by E. Arge, A. M. Bruaset, and H. P. Langtangen (Birkhäuser Press, 1997) pp. 163–202.
- [53] The number of foldings of the quasi-energy spectrum, for $L = 20$ at $\omega = 8$ is ~ 5 .
 - [54] D. N. Page, Physical review letters **71**, 1291 (1993).
 - [55] See supplementary information for details.
 - [56] The analytic ratio averages over all sites of a $L = 20$ open chain.
 - [57] The nature of the short time dynamics is dependent on both the operator considered and the truncation order of D_{eff} . Other operators are considered in detail in the supplementary information [55]. That there is a plateau at short times arises from the close relationship between $D_{\text{eff}}^{(0)}$ and $\mathcal{D}_{\text{eff}}^n$. As the systems thermalizes with respect to $\mathcal{D}_{\text{eff}}^n$, the expectation value of $D_{\text{eff}}^{(0)}$ will not change significantly as it approaches its thermal average $\langle D_{\text{eff}}^{(0)} \rangle_{\mathcal{D}_{\text{eff}}^n} = \text{Tr}(D_{\text{eff}}^{(0)} e^{-\beta_{\text{eff}}^n \mathcal{D}_{\text{eff}}^n})/Z$. The value of the plateau then corresponds to the difference in the thermal value of $D_{\text{eff}}^{(0)}$ calculated with respect to $\mathcal{D}_{\text{eff}}^n$ and the full D_{eff} . By varying n , one changes both the Hamiltonian to which the system thermalizes as well as the effective temperature of the prethermal regime β_{eff}^n , leading to a non-trivial dependence of the plateau value with both n and ω (but expected to monotonically decrease as either increases).
 - [58] D. Basko, I. Aleiner, and B. Altshuler, Annals of physics **321**, 1126 (2006).
 - [59] I. Gornyi, A. Mirlin, and D. Polyakov, Physical review letters **95**, 206603 (2005).
 - [60] D. A. Huse, R. Nandkishore, V. Oganesyan, A. Pal, and S. L. Sondhi, Physical Review B **88**, 014206 (2013).
 - [61] Y. Bahri, R. Vosk, E. Altman, and A. Vishwanath, arXiv preprint arXiv:1307.4092 (2013).
 - [62] A. Chandran, V. Khemani, C. Laumann, and S. L. Sondhi, Physical Review B **89**, 144201 (2014).
 - [63] R. Nandkishore and D. A. Huse, Annu. Rev. Condens. Matter Phys. **6**, 15 (2015).
 - [64] J. Zhang, P. Hess, A. Kyprianidis, P. Becker, A. Lee, J. Smith, G. Pagano, I.-D. Potirniche, A. C. Potter, A. Vishwanath, *et al.*, arXiv preprint arXiv:1609.08684 (2016).
 - [65] S. Choi, J. Choi, R. Landig, G. Kucsko, H. Zhou, J. Isoya, F. Jelezko, S. Onoda, H. Sumiya, V. Khemani, *et al.*, Nature **543**, 221 (2017).

Supplementary Information for Exponentially Slow Heating in Short and Long-range Interacting Floquet Systems

Francisco Machado¹, Gregory D. Meyer¹, Dominic Else², Chetan Nayak^{2,3}, Norman Y. Yao¹

¹*Department of Physics, University of California, Berkeley, CA 94720, USA*

²*Physics Department, University of California, Santa Barbara, CA 93106 USA*

³*Station Q, Microsoft Research, Santa Barbara, CA 93106-6105, USA*

CALCULATION OF D_{eff}

In this section we compute the prethermal effective Hamiltonian D_{eff} of our periodically driven system. This time-independent Hamiltonian is the approximate generator of stroboscopic time evolution until τ^* . We obtain D_{eff} by approximating the time evolution under one period, U_f , by a truncated Magnus expansion, leading to a representation of D_{eff} as a power series in the period of the drive $T = 2\pi/\omega$.

Consider the time evolution under the Hamiltonian described in Equation (1) of the main text:

$$H_\ell(t) = \begin{cases} \left(J \sum_{i < j} \frac{\sigma_i^z \sigma_j^z}{|i-j|^\alpha} + J_x \sum_{\langle i,j \rangle} \sigma_i^x \sigma_j^x + \sum_i h_x \sigma_i^x \right) + \left(\sum_i h_y \sigma_i^y + h_z \sigma_i^z \right) = D + E & \text{for } 0 < t < \frac{T}{2} \\ \left(J \sum_{i < j} \frac{\sigma_i^z \sigma_j^z}{|i-j|^\alpha} + J_x \sum_{\langle i,j \rangle} \sigma_i^x \sigma_j^x + \sum_i h_x \sigma_i^x \right) - \left(\sum_i h_y \sigma_i^y + h_z \sigma_i^z \right) = D - E & \text{for } \frac{T}{2} < t < T \end{cases}, \quad (\text{S1})$$

where $D[E]$ is the time [in]dependent component of $H_\ell(t)$. The term E can be thought of as a magnetic field with a square wave time profile in the \hat{y} and \hat{z} directions. As in the main text, we define the analogous short-range model $H_s(t)$ by truncating the Ising interaction to nearest and next nearest neighbor.

The evolution under a period can be succinctly written as:

$$U_f = \exp \left\{ -i \frac{T}{2} (D - E) \right\} \exp \left\{ -i \frac{T}{2} (D + E) \right\}. \quad (\text{S2})$$

U_f can now be cast as the exponential of an effective Hamiltonian:

$$U_f \approx \exp \{ -iT D_{\text{eff}} \} = \exp \left\{ -i \frac{T}{2} (D - E + D + E) + \frac{1}{2} \left(-i \frac{T}{2} \right)^2 [D - E, D + E] + \dots \right\} \quad (\text{S3})$$

Upon algebraic simplification and collection of terms, D_{eff} can be recovered as a sum of products of the terms D and E :

$$\begin{aligned} D_{\text{eff}} = & D + \frac{i}{2} \frac{T}{2} (ED - DE) - \frac{1}{6} \left(\frac{T}{2} \right)^2 (EED - 2EDE + DEE) \\ & + \frac{i}{24} \left(\frac{T}{2} \right)^3 [(EDDD + DEEE - EEED - DDDE) + 3(EEDE + DDED - EDEE - DEDD)] \\ & + \frac{1}{360} \left(\frac{T}{2} \right)^4 \left[-27(EDDED + DEDDE) + 23(DEEDE + EDEDD) + 18(EDDDE + EEDEE) + 8DEDED \right. \\ & \quad \left. - 12(EEEDE + EDEEE) - 7(EEDDD + DDDEE) + 3(DEEEE + EEEED) - 2(DEEDD + DDEED) \right] \\ & + \dots \end{aligned} \quad (\text{S4})$$

Although cumbersome, this formulation of D_{eff} provides a straightforward numerical implementation within the SLEPc and PETSc libraries [1–3] as one can obtain all orders of D_{eff} in terms of only D and E . Equation (S4) holds regardless of the form of its interacting terms, so it applies to both the short- and long-range models. As per the main text, we define $\mathcal{D}_{\text{eff}}^n$ as the truncation of D_{eff} to n -th order in $1/\omega$.

τ^* AS A FUNCTION OF INITIAL ENERGY DENSITY

The existence of a prethermal regime has been proven as an upper bound in the difference of time evolved operators under the full Hamiltonian and D_{eff} [4–6]. The generality of this approach leaves an open question: what is the effect of different initial

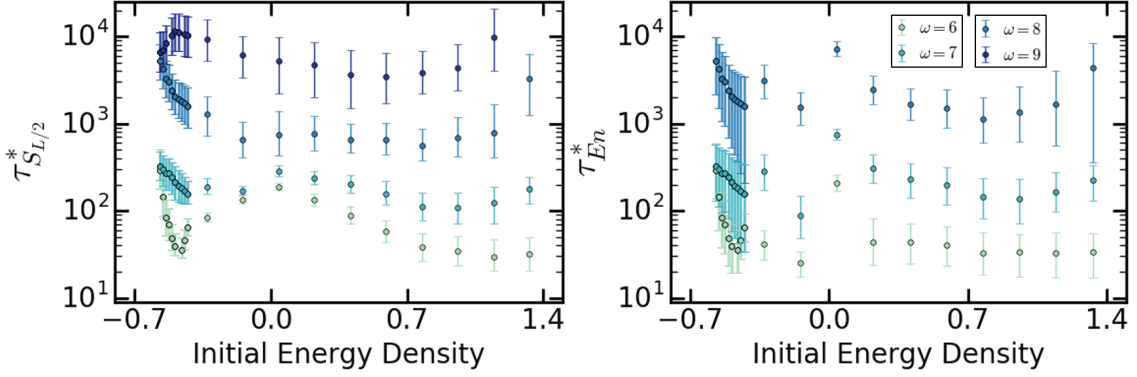


FIG. S1: τ^* of the short-range interacting model as a function of the energy density of the initial state (measured with respect to $D_{\text{eff}}^{(0)}$) and the frequency of the drive. **a)** τ^* as estimated using the entanglement entropy of the system. **b)** τ^* as estimated using the evolution of the energy density. In both cases we observe an overall independence on the initial state except near the center and edges of the spectrum, where we believe our estimation scheme and the change in density of states lead to the deviations, respectively.

states in the thermalization time scale of a system? In this section we attempt to shed some light onto this question by analyzing how the thermalization time scale, τ^* , changes as a function of energy density of the initial state (measured with respect to $D_{\text{eff}}^{(0)}$) for both short- and long-range interacting systems.

We estimate τ^* in two different ways - using the evolution of the entanglement entropy $S_{L/2}(t)$, and of the energy density $\langle \mathcal{D}_{\text{eff}}^{(2)} \rangle / L$. Firstly, we estimate τ^* to be the time when the entanglement entropy is half-way between its prethermal plateau $S_{L/2}^P$ and its final value of $(L \ln(2) - 1)/2$ [7]:

$$S_{L/2}(\tau^*) = S_{L/2}^P + \frac{1}{2} \left[\frac{(L \ln(2) - 1)}{2} - S_{L/2}^P \right]. \quad (\text{S5})$$

Given the large size of our system, we are unable to compute directly $S_{L/2}^P$ as a function of the initial energy density (since that would require full exact diagonalization). With this constraint, we instead estimate $S_{L/2}^P$ using the value $S_{L/2}(t)$ when we observe the system has reached a plateau at frequency $\omega = 9$:

$$S_{L/2}^P \approx S_{L/2}(t_{\text{pre}}), \quad (\text{S6})$$

where we have used $t_{\text{pre}} = 300, 200$ for the short- and long-range models respectively. Secondly, we estimate τ^* to be the time when the energy is half-way between its initial value and its infinite temperature value $\langle \mathcal{D}_{\text{eff}}^n(t) \rangle \rightarrow 0$:

$$\langle \mathcal{D}_{\text{eff}}(\tau^*) \rangle = \frac{\langle \mathcal{D}_{\text{eff}}(0) \rangle}{2}. \quad (\text{S7})$$

Equation (S7) contains an ambiguity as to which order one should consider for D_{eff} . Performing the analysis with different $\mathcal{D}_{\text{eff}}^n$, one observes no qualitative change in the results, so we choose $\mathcal{D}_{\text{eff}}^2$ for the remainder of this work.

We now analyze how τ^* varies for different initial states. We consider initial product states with spins polarized along \hat{z} and control the energy density by varying the number of equally spaced domain walls. In Figure S1, we consider τ^* for the short-range interacting system at different frequencies using both entanglement entropy, Figure S1(a), and energy density Figure S1(b). In both cases we observe the qualitatively similar behaviors. As a function of frequency, we observe an exponential dependence across the entire set of initial states, as expected from the state independent results proven in [4–6]. We also observe no large dependence on the energy density, except near the center and at the edges. For the former, the closeness of $S_{L/2}^P$ and the initial energy density to their infinite temperature values limits our ability to correctly estimate τ^* . For the latter, a lower density of states is expected to decrease the rate at which the system is able to absorb energy from the drive leading to an increase in τ^* , as highlighted in Figure 3b of the main text.

In Figure S2 we perform the analogous analysis for the long-range interacting system. Again we observe the same qualitative behavior when estimating τ^* using the entanglement entropy, Figure S2a, and the energy density, Figure S2b. Moreover, both short- and long-range interacting systems present the same overall qualitative features. We note, however, two important differences between the two. In the long-range model there is a more pronounced increase in τ^* near the edges of the spectrum. This is in agreement with our understanding that this phenomena arises as a density of states effect, since the long-range model has a smaller density of states near the edge of the spectrum. Moreover, the frequency has a smaller impact on τ^* in the long-range model across the entire spectrum, consistent with the results presented in Figure 3 for a few different initial states.

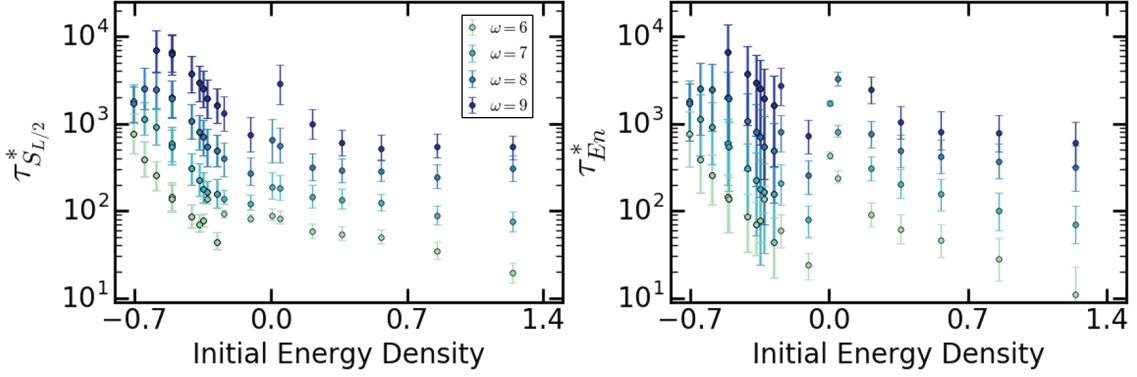


FIG. S2: τ^* of the long-range interacting model as a function of the energy density of the initial state (measured with respect to $D_{\text{eff}}^{(0)}$) and the frequency of the drive. **a)** τ^* as estimated using the entanglement entropy of the system $\tau_{S_{L/2}}^*$. **b)** τ^* as estimated using the evolution of the energy density τ_{En}^* . We observe the same qualitative behavior as in the short-range interacting model, depicted in Figure S1, but with a larger increase of τ^* at the edge of the spectrum and a smaller dependence with the frequency of the drive, in agreement with the analysis presented in Figure 3 of the main text.

ESTIMATING THE ENTANGLEMENT ENTROPY PLATEAU HEIGHT $S_{L/2}^P$

In this section, we describe a way to obtain $S_{L/2}^P$ (for $L = 20$) by estimating the entanglement entropy of $\mathcal{D}_{\text{eff}}^n$ on both short- and long-range models using exact diagonalization (ED) results from smaller system sizes, $L = 6, 8, 10, 12$. Having obtained the eigenspectrum of $\mathcal{D}_{\text{eff}}^4$ it becomes straightforward to both compute the energy density ϵ and $S_{L/2}$ of a thermal state of D_{eff} as a function of inverse temperature β :

$$L\epsilon(\beta) = \langle \mathcal{D}_{\text{eff}}^4 \rangle_\beta = \frac{\text{tr}(\mathcal{D}_{\text{eff}}^4 e^{-\beta \mathcal{D}_{\text{eff}}^4})}{Z} \quad \text{and} \quad S_{L/2}^P(\beta) = \text{Tr}(-\rho_{L/2}^\beta \ln \rho_{L/2}^\beta) \quad (\text{S8})$$

where $Z = \text{Tr}(e^{-\beta \mathcal{D}_{\text{eff}}^4})$ and ρ is the reduced density matrix defined as:

$$\rho_{L/2}^\beta = \text{Tr}_{i \leq 1 \leq L/2} \left(\frac{e^{-\beta \mathcal{D}_{\text{eff}}^4}}{Z} \right) \quad (\text{S9})$$

Having computed both $\epsilon(\beta)$ and $S_{L/2}^P(\beta)$ for different β , one obtains implicitly the entanglement entropy as a function of the energy density, $S_{L/2}(\epsilon)$, as illustrated in Figure S3. We have also included the limiting cases of zero and infinite temperature that corresponds to the edge and center of the spectrum ($\epsilon = 0$) respectively, where the entanglement entropy is $S_{L/2}^P = 0$ and $S_{L/2}^P = \frac{L}{2} \ln(2)$.

From these data, we construct a cubic extrapolation $s^{\text{est}}(\epsilon)$ of $S_{L/2}^P/(L/2)$. Given the small finite size effect of $S_{L/2}^P/(L/2)$ for $\epsilon < 0$ we assume that $s^{\text{est}}(\epsilon < 0)$ remains constant as we vary the system size. For $\epsilon > 0$, increasing the system size leads to an increase in the width of the spectrum. As a result, in order to use $S_{L/2}$ at system size $L' = 12$ to estimate $S_{L/2}$ at system size $L = 20$, we need to rescale the energy density before using our interpolation. The resulting estimate for $S_{L/2}^P$ is given by:

$$S_{L/2}^{\text{Est}} = \frac{L}{2} \times s^{\text{est}} \left(\frac{\epsilon_L}{\epsilon_L^{\text{max}}} \epsilon_{L'}^{\text{max}} \right), \quad (\text{S10})$$

where ϵ_L is the initial energy density in the $L = 20$ state, while ϵ_l^{max} is the edge of spectrum at system size l . In the case of $l = L$, we consider the energy density of the fully polarized state, while in $l = L'$ it can be obtained exactly from ED. This rescaling serves two purposes: 1) ensuring that the argument falls inside the domain of the interpolation, and 2) attempting to account for finite size effects. From Figure S3 we observe that a smaller L leads to a larger slope near the edge of the spectrum. This leads to an overestimation of $S_{L/2}^P$ in the long-range case as observed in our results. Finally, since we are evolving a pure initial state unitarily, the system will never reach the true thermal ensemble, leading to a correction of 0.5 in Equation (S10) [7]:

$$S_{L/2}^{\text{Est}} = \frac{L}{2} \times s^{\text{est}} \left(\frac{\epsilon_L}{\epsilon_L^{\text{max}}} \epsilon_{L'}^{\text{max}} \right) - 0.5 \quad (\text{S11})$$

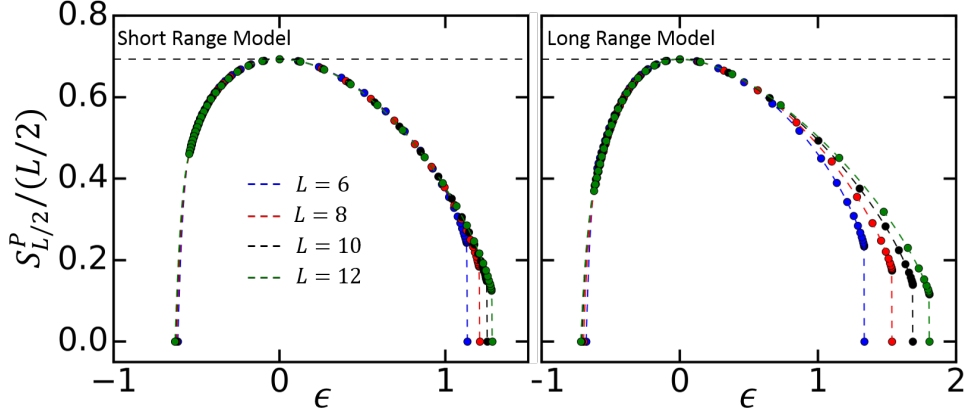


FIG. S3: **a[b]** Half-chain entanglement entropy density $S_{L/2}/(L/2)$ as a function of the energy density ϵ of the thermal state of the short-[long-]range model and for different system sizes $L = 6, 8, 10, 12$. Dashed line corresponds to a cubic interpolation to the data points. For negative energy density, $S_{L/2}/(L/2)$ is approximately constant as a function of system size for both short- and long-range models. However, for positive ϵ , there is a large size effect for the long-range model, which limits the validity of our extrapolation.

ESTIMATING ERRORS IN THE NUMERICS

In order to quantify our uncertainty in the extraction of quantities from our numerics we define the following procedures as our uncertainty.

- τ^* - The extraction of τ^* depends on the estimation of $S_{L/2}^P$. Due to the simple method considered in Equation (S6) we consider our uncertainty regime in τ^* as:

$$S_{L/2}(\tau_{min}^*) = S_{L/2}^P + 0.35 \times \left[\frac{(L \ln(2) - 1)}{2} - S_{L/2}^P \right]; \quad S_{L/2}(\tau_{max}^*) = S_{L/2}^P + 0.65 \times \left[\frac{(L \ln(2) - 1)}{2} - S_{L/2}^P \right]. \quad (\text{S12})$$

We estimate our error as the maximum deviation between $|\tau^* - \tau_{min}^*|$ and $|\tau^* - \tau_{max}^*|$. In the case of the extraction of τ^* from the energy density we apply the same criterion.

- m_{δ_n} - The uncertainty in this quantity arises from the impact of the plateau physics, that can change the fit to a straight line, as well as the choice of the region where we observe the linear regime. We account for these phenomena by dividing the range where we observe the linear effect into six equally sized sub regions. By applying the fit within each of the regions, we obtain an estimate of m_{δ_n} . While the true estimate becomes the average of these values, we take the uncertainty as the 2σ standard deviation.
- h_p^n - Similar to m_{δ_n} we define a region where we observe the existence of the plateau. h_p^n is then given by the average of the δ_n at these points, while we take the uncertainty as the 2σ standard deviation.

PRETHERMAL EFFECTIVE HAMILTONIAN FOR SHORT-RANGE INTERACTING SYSTEM

In Figure 4 of the main text, we analyzed the role of D_{eff} as the approximate generator of stroboscopic time evolution for the long-range interacting model. In this section we supplement those results by studying the short-range model using $\mathcal{O} = D_{\text{eff}}^{(0)}/L$ as well as considering other local operators in both short- and long-range models. Analogous to the results presented in Figure 4 of the main text, we consider the difference δ_n in the expectation value of $\mathcal{O} = D_{\text{eff}}^{(0)}/L$ when time evolved under $\mathcal{D}_{\text{eff}}^n$ or the full Floquet unitary in the short-range interacting model with $L = 16$.

In Figure S4a we observe the same qualitative behavior as in the long-range interacting system analyzed in the Figure 4a of the main text. In particular we observe the same initial plateau originating from the difference between $\mathcal{D}_{\text{eff}}^n$ and D_{eff} as well as the late time linear regime. Immediately, one notices that for the same range of frequencies, the linear regime of δ_n occurs at later times corresponding to a slower linear growth. In Figure S4b,c we quantify these aspects by analyzing the frequency dependency of both the slope of the linear regime, and the height of the plateaus. From the linear slope, we extract an effective interaction strength $J_{\text{eff}}^s = 0.6 \pm 0.1$ which is in agreement with the results from the analysis presented in Figure 3 in the main

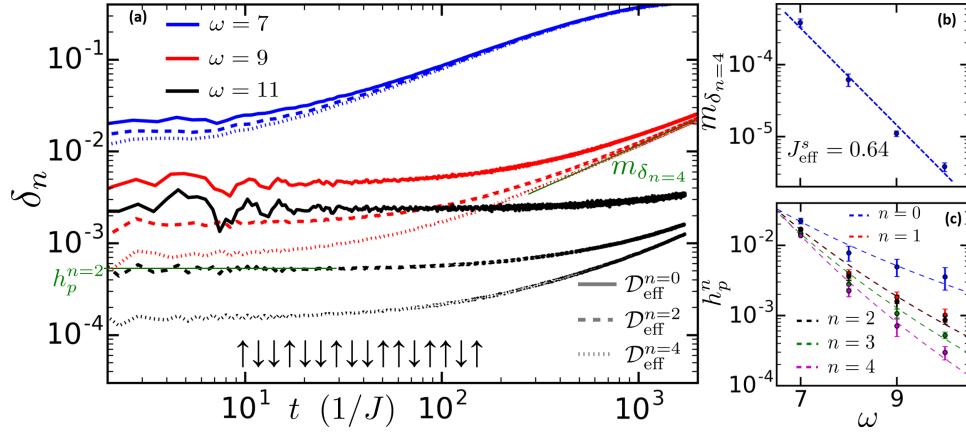


FIG. S4: a) The difference, δ_n , of the expectation value of $\mathcal{O} = D_{\text{eff}}^{(0)}/L$ as a function of time, for a chain of length $L = 16$ with short-range interactions, with different frequencies (colors) and different Magnus truncation orders (line style). The distinct regimes are seen: an initial plateau at short times and a linear increase at late times. b) Extracted slope of the late time linear regime of δ_n as a function of frequency. This provides an independent estimate for J_{eff}^s which is in agreement with that calculated from $\tau_{S_{L/2}}^*$, in Figure 3 of the main text. c) Plateau height $h_{pl}^{(n)}$ for different Magnus truncation orders, n , as a function of frequency. The results are consistent with an n -dependent power law.

text, $J_{\text{eff}}^s = 0.5 \pm 1$. Regarding the plateau height we observe a similar power law dependence with frequency $h_p \sim \omega^{-\eta}$ as in the long-range case, but with larger values of η .

We now demonstrate that the results presented in Figure 4 and Figure S4 extend to other local operators of the system. In particular we will consider the operators σ_i^z , σ_i^x , $\sigma_i^z \sigma_{i+1}^z$ and $\sigma_i^x \sigma_{i+1}^x$ at site i , by measuring the errors $\delta_i^z, \delta_i^x, \delta_i^{zz}$ and δ_i^{xx} respectively, defined between time evolution under D_{eff}^n and the full Hamiltonian. We then define $\overline{\delta^z}, \overline{\delta^x}, \overline{\delta^{zz}}$ and $\overline{\delta^{xx}}$ as the average of the errors over the all sites of the chain. In analogy to Figure 4 and Figure S4, we observe the emergence of a late time linear regime for all the considered operators, as shown in Figure S5 (short-range) and Figure S6 (long-range). The rate of growth of the linear regime decreases both with increasing n and ω , consistent with D_{eff} being the approximate generator of time evolution. However, unlike the case when $\mathcal{O} = D_{\text{eff}}^{(0)}/L$, the early time behavior has a more complex structure. In these cases, we do not expect these local operators to be approximately conserved, so we observe different, operator dependent, thermalization dynamics.

To corroborate that the early time behavior is due to differences in short-time thermalization dynamics, we estimate $\tau_{D_{\text{eff}}}$ as the time, the system approaches $S_{L/2}^P$. After this time, we observe that most of the error is given by an initial plateau followed by a linear regime. For $t > \tau_{D_{\text{eff}}}$, extracted in Figure S7, the system has thermalized to D_{eff} , so the error is dominated initially by the difference the thermal expectation of \mathcal{O} with respect to D_{eff} or D_{eff}^n , until the linear growth in error from the difference between D_{eff} and the full evolution dominates.

Finally, we emphasize that the agreement we observe for the long-range model in Figure S6 between the evolution under the full Hamiltonian and the different orders of D_{eff} at different frequencies provides further evidence of the existence of a prethermal effective Hamiltonian given by D_{eff} that approximately describes the time evolution of our system, even though no formal proofs exist for power-law interactions at present.

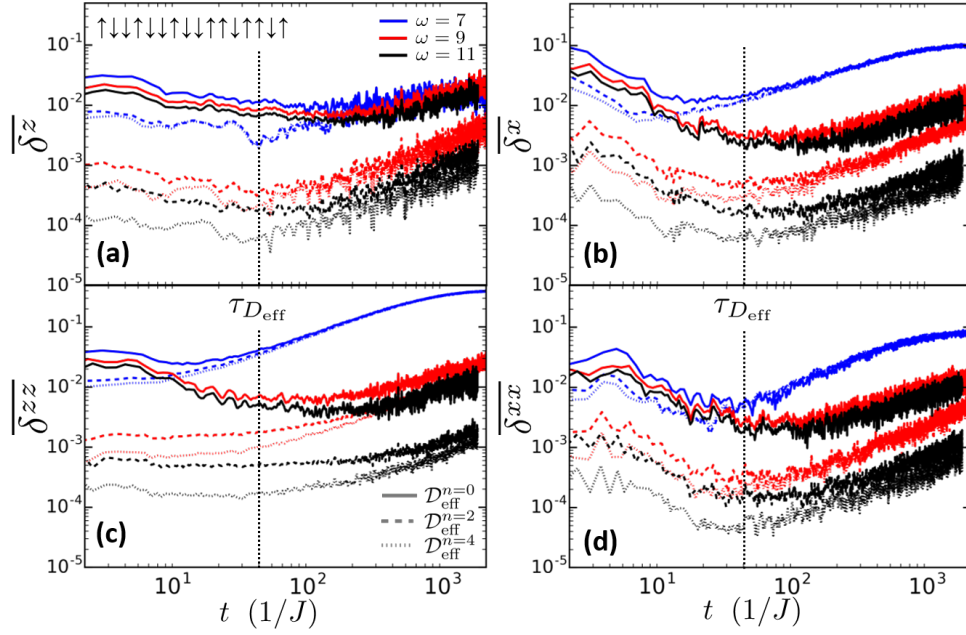


FIG. S5: Difference in local operators, $(\sigma_i^z$ [a], σ_i^x [b], $\sigma_i^z \sigma_{i+1}^z$ [c], $\sigma_i^x \sigma_{i+1}^x$ [d]) when evolved under the full evolution and $\mathcal{D}_{\text{eff}}^n$ of the short-range model. Similar to Figure 4 and Figure S4 we observe a late time linear regime, corresponding to the linear accumulation of error. At early times we observe a complex behavior arises from the thermalization dynamics to $\mathcal{D}_{\text{eff}}^n$. For $t > \tau_{D_{\text{eff}}}$, as extracted from Figure S7, the error follows the same behavior as in Figure 4a and Figure S4a when $\mathcal{O} = D_{\text{eff}}^{(0)}/L$. Despite the initial behavior, an increase in n leads to an earlier onset of the linear regime, as expected from D_{eff} being the approximate generator of time evolution, consistent with previous theoretical results.

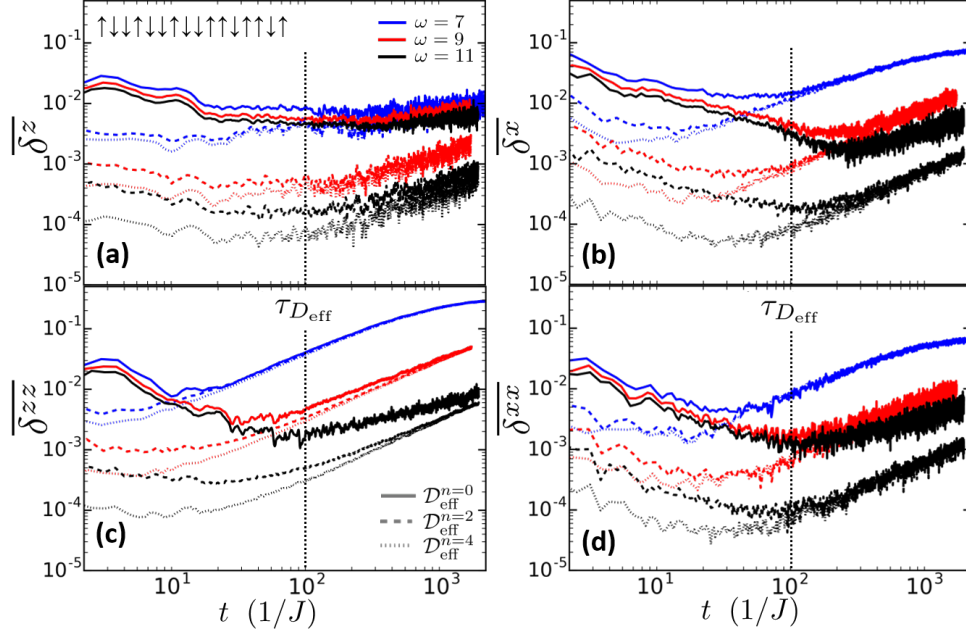


FIG. S6: Difference in local operators, $(\sigma_i^z$ [a], σ_i^x [b], $\sigma_i^z \sigma_{i+1}^z$ [c], $\sigma_i^x \sigma_{i+1}^x$ [d]) when evolved under the full evolution and $\mathcal{D}_{\text{eff}}^n$ of the long-range model. We observe a qualitatively similar picture to the results presented in Figure S5. This provides further evidence of D_{eff} being the approximate generator of stroboscopic time evolution. Similarly to Figure S5, the error dynamics becomes simpler for $t > \tau_{D_{\text{eff}}}$, as extracted from Figure S7.

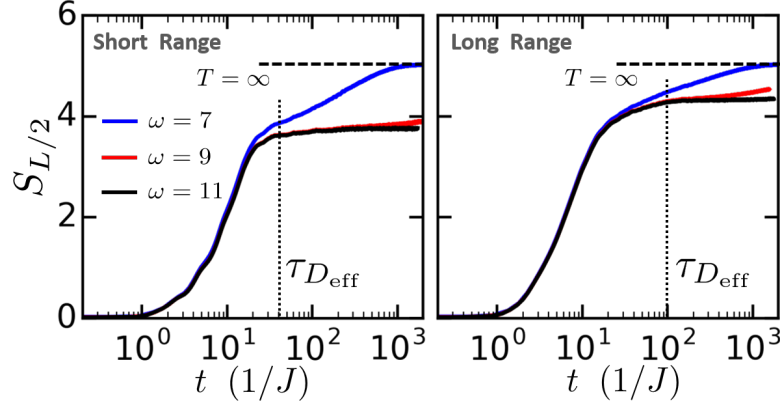


FIG. S7: **a[b]**) Entanglement Entropy evolution for the full Hamiltonian for short-[long-] model. The thermalization of the system with respect to D_{eff} leads to the emergence of a plateau in the entanglement entropy. We define the time at which this plateau begins as $\tau_{D_{\text{eff}}}$. We estimate this time scale for short- and long-range models as $\tau_{D_{\text{eff}}}^s = 40$ and $\tau_{D_{\text{eff}}}^l = 100$ respectively.

For the data presented in Figure 2 of the main text, we focused on antiferromagnetic product states, where heating manifests as an increase in the energy density toward its infinite temperature value (namely, zero). In the case of ferromagnetic states, the process of heating actually corresponds to a decrease in the value of $\langle D_{\text{eff}}^{(0)} \rangle / L$. As shown in Figure S8 for a chain of $L = 22$, one observes an exponential enhancement of the thermalization time from an initial state on the ferromagnetic side of the spectrum.

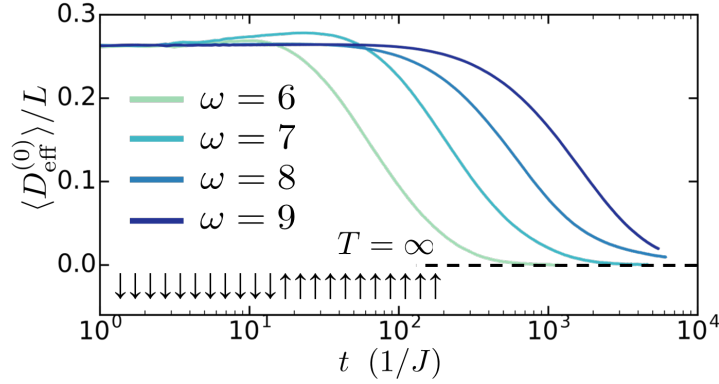


FIG. S8: Exponentially long thermalization dynamics for $L = 22$ spins using an initial state on the ferromagnetic side of the spectrum. The process of heating toward the infinite temperature thermal ensemble actually shows up as a decrease of the energy density toward zero.

-
- [1] V. Hernandez, J. E. Roman, and V. Vidal, *ACM Trans. Math. Software* **31**, 351 (2005).
 - [2] J. E. Roman, C. Campos, E. Romero, and A. Tomas, Tech. Rep. DSIC-II/24/02 - Revision 3.7, D. Sistemes Informàtics i Computació, Universitat Politècnica de València (2016).
 - [3] S. Balay, W. D. Gropp, L. C. McInnes, and B. F. Smith, in *Modern Software Tools in Scientific Computing*, edited by E. Arge, A. M. Bruaset, and H. P. Langtangen (Birkhäuser Press, 1997), pp. 163–202.
 - [4] D. A. Abanin, W. De Roeck, and F. Huveneers, *Physical review letters* **115**, 256803 (2015).
 - [5] D. Abanin, W. De Roeck, W. W. Ho, and F. Huveneers, *Communications in Mathematical Physics* pp. 1–19 (2015).
 - [6] D. V. Else, B. Bauer, and C. Nayak, *Physical Review X* **7**, 011026 (2017).
 - [7] D. N. Page, *Physical review letters* **71**, 1291 (1993).